Article

Terahertz Waves Enhance the Permeability of Sodium Channels

Yan Zhao [1], Lei Wang [1], Yangmei Li [2],* and Zhi Zhu [1],*

[1] Key Laboratory of Optical Technology and Instrument for Medicine, Ministry of Education,
College of Optical-Electrical and Computer Engineering, University of Shanghai for Science and Technology,
Shanghai 200093, China
[2] Innovation Laboratory of Terahertz Biophysics, National Innovation Institute of Defense Technology,
Beijing 100071, China
* Correspondence: sunberry1211@hotmail.com (Y.L.); zhuzhi@usst.edu.cn (Z.Z.)

Abstract: With the help of molecular dynamics simulations and an artificial sodium channel model, we corroborated that the application of terahertz stimulation at a characteristic frequency can largely increase the permeability of the sodium channel by a factor of 33.6. The mechanism is that the carboxylate groups in the filter region transfer the absorbed terahertz photon energy to the sodium ions, which increase the ions' kinetic energy; this results in breaking the hydrated hydrogen bonding network between the hydrosphere layer of the ions and the carboxylate groups, thereby increasing their diffusion and reducing the energy barrier for them to cross the channel. This study on terahertz-driven particle transmembrane transport offers new ideas for targeted therapy of channel diseases and for developing novel integrated engineering systems in energy conversion and storage.

Keywords: ion channel; molecular dynamic simulation; particle transport; vibration spectrum

1. Introduction

Sodium ions, as one of the main metal elements in living organisms, play an integral role in the regulation of cellular functions, such as the maintenance of endocrine cell excitability, cell membrane permeability [1], and the correct conduction of electrical impulses in the heart [2]. Therefore, sodium channels as carrier proteins are among the popular research subjects. Its unique osmotic selectivity allows it to be used in wastewater treatment [3] and desalination [4,5]. In addition, its permeability can direct the generation of bioelectric phenomena, bringing cells from resting potentials to action potentials, which helps to study sodium channel diseases in medical clinics due to sodium potential dysregulation as well as genetic mutations. Examples include critical illness polyneuropathy [6], minimal change disease-related nephrotic syndrome [7], conduction disorders and ventricular arrhythmias [2,8,9], neurological disorders—primary red-hot pain sympathetic dysfunction [10], and many others. These facts indicate that reduced sodium permeability is a major factor in triggering these diseases. Therefore, it is essential to have a clear idea of the sodium permeability process, which also contributes to the interventions for the treatment of such diseases.

The permeation and selection mechanisms of sodium channels originate from the interaction between Na^+ ions and charged functional groups ($-COO^-$) in the selective filter region of the channels [11,12] and most low-frequency biomolecular motions are in the same frequency range as terahertz and infrared signals [13–16]. The frequency region from 0.5 to 100 THz thus was named as the generalized terahertz EM wave [17]. Terahertz waves can interfere with the activity of biological systems [18–20], and significant non-thermal biological [21,22] and thermal [23] effects occur. For example, terahertz waves significantly interfere with the naturally occurring local strand separation of double helix DNA [24], thereby altering functions such as DNA gene expression [25,26]. Electromagnetic (EM) stimulation at the frequency of 1.39 THz induces super-permeability of confined water

(approximately one order of magnitude) and a phase transition from a one-dimensional ice phase to a one-dimensional coherent gas phase [27], while EM stimulation at the frequency of 31.5 ± 1.0 THz induces a 37-fold increase in the super-permeability of confined mono-layer water through a graphene-based membrane [28]. EM stimulation of 35.0 ± 1.0 THz resonates with the vibration of hydroxyl groups on graphene oxide membranes (GO membranes) and transfers its photon energy to the membrane, resulting in a 141-fold increase in the permeability of GO membranes [29]. High-frequency terahertz (e.g., 53.7 THz) stimulus resonates with carbonyls in the filter region of potassium channels to increase K^+ currents, further regulating brain function and treating brain diseases [30], and correcting tumor cells with reduced potassium currents or causing rapid apoptosis of potassium overload [31]. EM stimulation of 42.55 THz on calcium channels can result in significant enhancement of calcium ions selectivity and conductance, thus correcting for reduced calcium currents in defective Ca^{2+} channels or inducing rapid apoptosis in calcium-overloaded tumor cells [32,33]. EM stimulation of 4.0 THz can increase the dissociation rate between dopamine D2 receptors and risperidone ligands by up to 8 orders of magnitude in pharmacological interventions for disease treatment, thereby facilitating the dissociation of high-affinity antipsychotics and reducing side effects [34]. Terahertz waves at certain specific frequencies in single-walled carbon nanotubes cause hydrogen bond breakage through rotation and rotation-induced translational resonance [35] or through their radial breathing mode [36], which in turn leads to a threefold enhancement in the net flux of water. Inspired by the above studies, we wondered whether EM stimulation at a specific frequency could change the permeability of sodium channels.

In this study, we propose a physical method to enhance the permeability of sodium channels by modulating the carboxylate groups (-COO^-) inside the sodium channel with THz stimulation (Figure 1a), and find out that the value of ion permeation in the case under 48.2 THz EM stimulation is 33.6 times greater than the one under the normal permeability state (Figure 1b), which is much more effective than the approach of temperature elevating. The underlying mechanism is resonance-driven energy transfer, meaning that due to the frequency matching, terahertz photon's energy is transferred to the -COO^-, boosting the kinetic energy of the -COO^-, which then transfers energy to the Na^+ ions and reduces the binding of the -COO^- to the Na^+ ions through mutual collisions with Na^+ ions and water molecules.
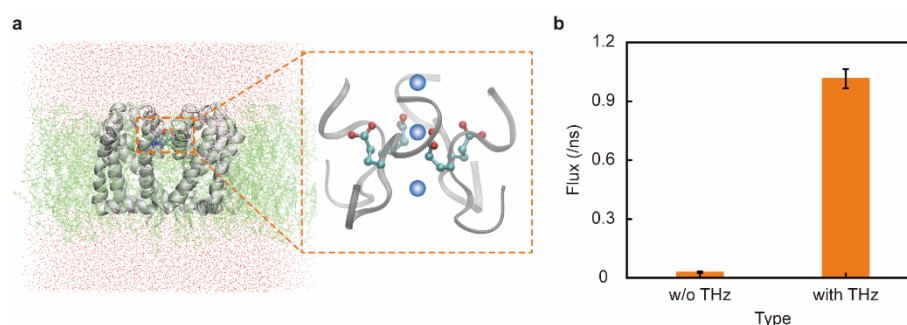
Figure 1. Schematic representation of the accelerated passage of sodium ions through the sodium channel under terahertz electromagnetic (EM) stimulus. (**a**) Schematic representation of a sodium channel protein, with the enlarged section showing the channel-selective filter region, the four carboxylate groups (-COO^-) of the four Glu amino acids. (**b**) Effect of adding a 48.2 THz EM wave on artificial sodium channels. The flow rate of the sodium channel was significantly increased by 33.6 times after the THz EM stimulation.

2. Method

According to the data of the crystal structure (PDB ID code 3RVY), the sodium channel embedded between the bilayer lipid membrane is composed of a quaternary arrangement of protein chains as well as a narrow pore region acting as a selective filter. Four -COO^- of anion residues in this pore region were proved to be the functional groups in determine

the ion-selective permeability of sodium ion channels [37]. Therefore, based on the real channels described above, we constructed a biologically inspired physical model of a sodium channel, where four -COO$^-$ were modified on the inner wall of a carbon nanotube in the same plane (as shown in Figure S1). The length and diameter of the nanotube are 0.485 and 0.535 nm, respectively. Furthermore, two graphene sheets were used to reproduce the function of bilayer lipid membranes to separate molecules. The software used for molecular dynamics simulations (MD) is GROMACS 2020 [38,39]. The detailed simulation parameters can be found in Section 1.a of the Supporting Information. We used an umbrella sampling method [40,41] to calculate the potential of the mean force (PMF) or free energy profile [42] of Na$^+$ ions during permeation of the pore selective filter, as detailed in Section 1.c of the Supporting Information. This PMF is obtained by integrating the average force sampled on the ion pathway with the help of a bias potential, which describes the energy relationship between the ions and the surrounding molecules during permeation. In the presence of an EM field, the motion of charged particles at room temperature depends mainly on the electric component of the EM wave [28], so we use only the electric field component $E(t) = A \cdot u \cdot \cos(\omega t + \varphi)$ as the EM stimulation. Here A, ω, and φ are the electric field strength, the angular frequency, and the initial phase, respectively. The direction of polarization of the wave is perpendicular to the plane of the membrane, i.e., $u = (0, 0, 1)$.

3. Results and Discussion

Figure 2 shows that a characteristic frequency of EM stimulation at 48.2 THz can distinctively improve the ion permeability of the biomimetic sodium channel. We characterized the permeability of ions in the channel in terms of the flow of ions (F), which describes the average number of ions permeating from one side of the channel to the other per nanosecond. First, we found that under EM stimulation at the characteristic frequency of 48.2 THz, the permeability of the sodium channel changed from normal permeability ($F = 0.03 \pm 0.01$ /ns) to ultrafast permeability ($F = 1.01 \pm 0.05$ /ns) as the stimulus strength A increased. However, with EM stimulation at other frequencies such as 36.0 THz, the permeation of Na$^+$ ions did not change significantly even when A reached an intensity of 1.0 V/nm (Figure 2a). Notably, the permeability of the channel remained at the normal permeability state when $A \leq 0.2$ V/nm and rapidly increased in a nonlinear way to 33.6-fold greater than the normal one when strength A increased from 0.2 to 1.0 V/nm, and after $A > 1.0$ V/nm, the permeability reached a plateau and remained stable. This fact suggests that the osmotic shift induced by EM stimulation occurs at specific frequencies, such as 48.2 THz. To emphasize the significance of the increased permeability caused by the EM stimulation, we investigated the relationship between ion permeation and temperature in the absence of EM stimulation (Figure 2b). By changing the temperature of the system, we found that the flow of Na$^+$ increases in a linear way with the elevation of temperature (from 293 K to 320 K), which follows the Einstein-Smoluchowski diffusion equation [43,44]. Although the F increased to 0.06 ± 0.01 /ns at 320 K, it was still much lower than the ultrafast permeation induced by 48.2 THz EM stimulation. As a result, the permeability of biomimetic sodium channels can be increased with light at particular frequencies.

To further investigate how light at specific frequencies enhances the permeability of the sodium channel, we analyzed the absorption spectrum of the -COO$^-$ in the sodium channel as well as the absorption spectrum of bulk water in the system (Figure 3). Different atoms or molecules are usually able to produce different fingerprint peaks in the spectrum. Therefore, we used the velocity and charge of an atom to obtain the absorption spectrum through the Fourier transform of its autocorrelation function [45–47]. As shown in Figure 3a, the -COO$^-$ in the sodium channel have characteristic absorption peaks at 9.4, 16.9, and 48.2 THz, in good agreement with the experimental -COO$^-$ spectral data [48]. The first two of these absorption peaks correspond to symmetric stretching vibrations of -COO$^-$ (lower intensity) [32]. To ensure that the EM wave penetrates the protein and avoids absorption by water, we also calculated the absorption bulk water spectrum. The first two absorption

frequencies of -COO$^-$ were found to be strongly absorbed by water and difficult to use as a resonance source. In contrast, the photon energy of 48.2 THz EM stimulation can be resonantly absorbed by the -COO$^-$, inducing the -COO$^-$ to enter the excited state and be able to produce a transfer of energy [49]. To confirm this conjecture, we compared the energy transfer of -COO$^-$, Na$^+$ ions, and water molecules in the presence and absence of 48.2 THz EM stimulation (Figure 3b–d). We discovered that, in the channel, the average kinetic energy E_k of the -COO$^-$ in the ultrafast permeability state (1.44 kcal/mol) was 1.60 times higher than the one in the normal permeability state (0.89 kcal/mol). Similarly, in the ultrafast permeability state, the energy of Na$^+$ (1.17 kcal/mol) was also greater than that in the normal permeability state (0.88 kcal/mol), agreeing with the increased diffusion coefficient (Figure S2). In addition, we compared the changes in the average kinetic energy among -COO$^-$, Na$^+$ ions, and water molecules at different A (Figure 3e). The kinetic energies of -COO$^-$, Na$^+$, and water molecules all showed a similar trend of increase as the strength A gradually increased. However, at the same intensity, the kinetic energy of the -COO$^-$ was always greater than that of the Na$^+$ ions, and the E_k of the Na$^+$ ions was greater than that of water. These results suggest that the -COO$^-$ in the channel increased their kinetic energy after absorbing the energy of 48.2 THz EM stimulation, thereby increasing the collisions of -COO$^-$ with Na$^+$ ions and water molecules; this further improves the process of kinetic energy transfer, causing a potential change in the interaction among them and accelerating the permeation of the sodium channel.
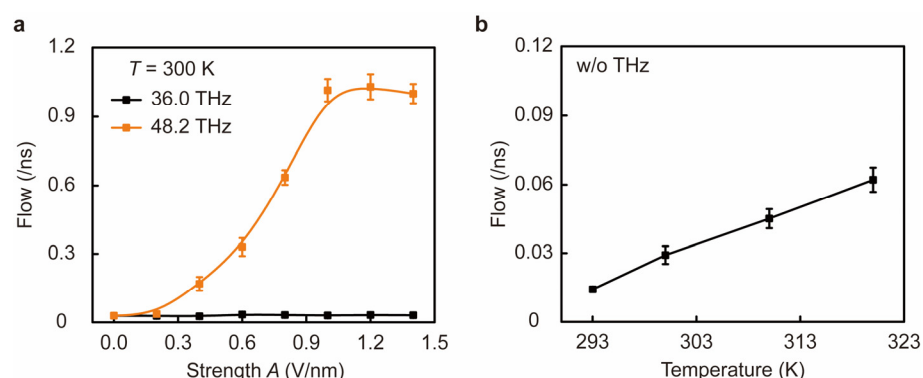
Figure 2. Effect of EM stimulation and temperature on the permeability of Na$^+$ ion channels. (**a**) Na$^+$ reaches an ultrafast permeability state as the stimulus strength (A) of 48.2 THz EM increases (orange curve); in contrast, the permeability of Na$^+$ remains in a normal permeability state under 36.0 THz EM stimulation (black curve). (**b**) In the absence of EM stimulation, the flow of Na$^+$ (the number of ions per nanosecond through the channel) increases with increasing ambient temperature T.

To uncover the pathway of energy transfer from the -COO$^-$ to Na$^+$ ions, we studied the effect of EM stimulation on the hydrogen bond (H-bond) network between -COO$^-$ and the hydrated layer of Na$^+$ (Figure 4a). It is important to clarify that sodium ions need to be encapsulated by a water shell layer throughout the permeation process [50]. The number of hydration coordination sites was 5~6 (Figure S3), which is consistent with the experimental results [37]. Na$^+$ ions will interact with the -COO$^-$ in the selective filter region of the channel so that -COO$^-$ acts as a compensation for shedding some of the water molecules, which is an important reason why -COO$^-$ can regulate Na$^+$ permeation [12]. Furthermore, H-bonds are formed between two molecules when the O-O distance is less than 0.35 nm and their H-bond angle is less than 30° [51,52]. Accordingly, Na$^+$ passing through the ligated hydrosphere will form H-bonds with the -COO$^-$ in the channel. Figure 4a elucidates that the -COO$^-$ affects Na$^+$ through hydrogen bonding, altering the permeation of Na$^+$ ions, regardless of the presence or absence of EM stimulation. Under the normal permeability state, water molecules in the aqueous shell layer of Na$^+$ ions form 1.90 H-bonds with the -COO$^-$ at the opening of the tube, which gradually decreases to 1.19 as the Na$^+$ ions penetrate deeper into the channel, due to the disruption of the aqueous shell layer

of ions in the channel. When the ions reach the position where the -COO⁻ are located (z = 0.0 Å), the -COO⁻ will have a compensating effect on the aqueous shell layer and form 1.90 H-bonds with the water molecules inside the channel. This fact also proves that, at this position, the Na⁺ ions are more easily trapped by the -COO⁻ and less likely to escape the channel, resulting in blocked permeation. However, after the application of 48.2 THz EM stimulation, the H-bonds are disrupted through collisions between the -COO⁻ and Na⁺ ions as well as the surrounding water spheres, and their average H-bond number ($N_{\text{H-bonds}}$) was significantly reduced, which explains the weakened energy transfer between the -COO⁻ and Na⁺ ions. Furthermore, during the entry of Na⁺ ions into the channel, the difference between the local maximum and minimum number of hydrogen bonds in the case with EM stimulation (ΔN_{with}) increases to 1.32 (in the case without stimulation $\Delta N_{w/o}$ = 0.79), enhancing the binding of Na⁺ to the -COO⁻. This fact further confirms that Na⁺ ions that can enter the channel faster can similarly be freed from -COO⁻ more easily, thereby facilitating the diffusion of Na⁺ ions and accelerating osmosis.
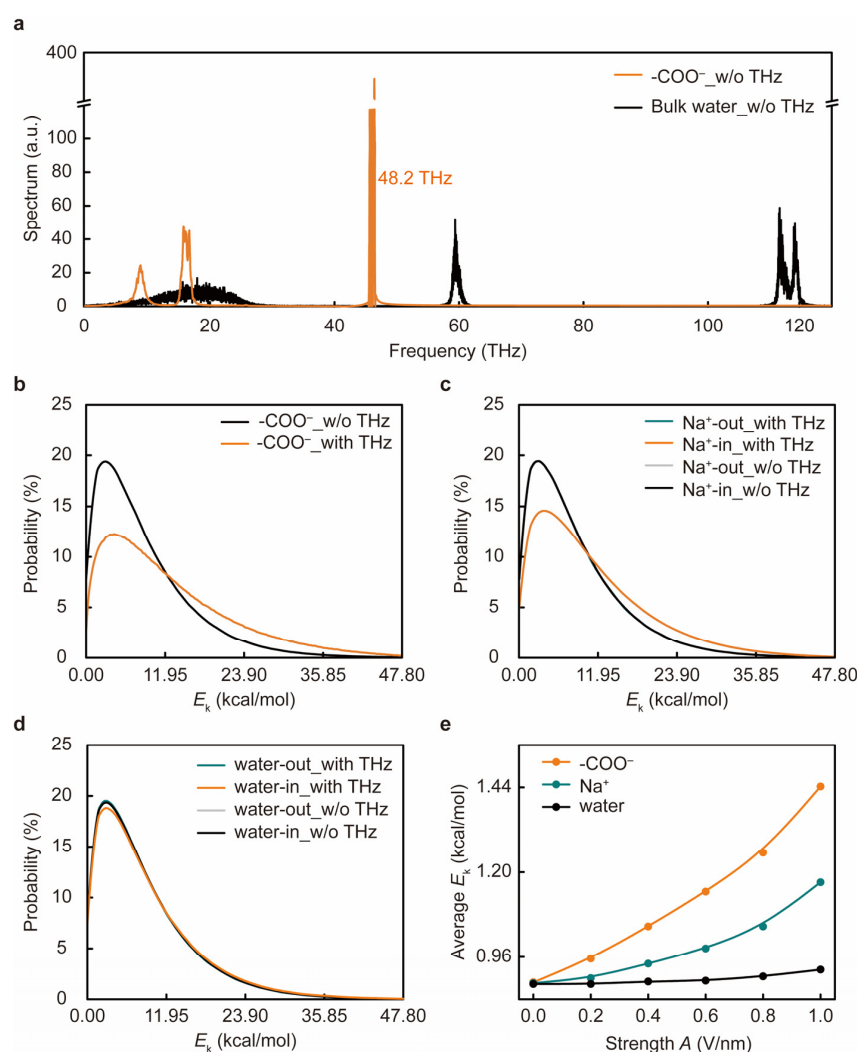
Figure 3. Vibrational spectra for -COO⁻ and bulk water inside the channels, and kinetic energy boosting and transferring process among -COO⁻, Na⁺ ions, and water in the channel. (**a**) Vibrational spectra of the -COO⁻ (orange curve) and bulk water (black curve) inside the channels. The main vibration frequencies (v_{main}) of -COO⁻ inside the channel are 9.4, 16.9, and 48.2 THz; the v_{main} of bulk water is 17.5 THz with a broad peak width. (**b–d**) Probability distributions of the molecular kinetic energy E_{k} of -COO⁻ (**b**), Na⁺ ions (**c**), and water (**d**) inside the sodium channel in the presence and absence of 48.2 THz EM stimulation. (**e**) Mean kinetic energy changes of -COO⁻, Na⁺ ions, and water with the application of 48.2 THz EM stimulation at different strengths A.
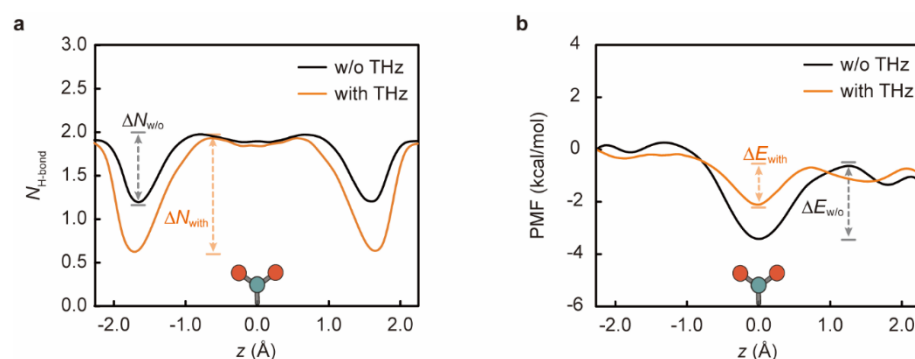
Figure 4. The average number of hydrogen bonds ($N_{\text{H-bond}}$) between water and -COO$^-$ in the first water shell layer of Na$^+$ and the distribution of free energy profiles of Na$^+$ permeating along the z-direction of the channel in the presence and absence of 48.2 THz EM stimulation. (**a**) The maximum $N_{\text{H-bond}}$ in the case without EM stimulation was 1.98 (black curve), while it decreased to 1.92 after the addition of 48.2 THz EM stimulation (orange curve). Moreover, the difference between the local maximum and minimum number of hydrogen bonds in the case with EM stimulation (ΔN_{with}) is 1.32, while it is 0.79 in the case without the stimulation ($\Delta N_{w/o}$). (**b**) The z on the x-axis denotes the distance of the ion from the center point of the channel in the z-direction throughout the traction process. The difference of Na$^+$ between the potential at the local maximum point in the direction of the channel exit and the potential at the minimum point is 2.79 kcal/mol for the case without EM stimulation ($\Delta E_{w/o}$), while the energy barrier difference is 1.52 kcal/mol for the case with the stimulation (ΔE_{with}), denoting an accelerated Na$^+$ penetration. The icon at $z = 0.0$ Å represents the position of -COO$^-$; the two red spheres are the oxygen atoms and the green one is the carbon atom.

Finally, we performed calculations of the potential of the mean force (PMF) of Na$^+$ ions in the cases with and without the addition of 48.2 THz EM stimulation. It is able to reflect the free energy change of the ions passing through the channel [42,53,54]. Figure 4b shows the PMF results for Na$^+$ passing through the channel in the presence and absence of 48.2 THz EM stimulation. As the distance between the Na$^+$ and the -COO$^-$ decreases, the energy potential trap gradually increased, indicating that the interaction force between them is also gradually intensifying, corresponding to the enhancement in the number of H-bonds in Figure 4a. Moreover, with the application of 48.2 THz EM stimulation, the energy consumed by the Na$^+$ to reach the filter region of the channel ($z = 0.0$ Å) is less than that in the normal permeability state, which indicates that the Na$^+$ can enter the channel more easily. In addition, the free energy difference between the potential at the highest local point in the direction of the channel exit and the lowest potential ($\Delta E_{w/o}$) is relatively high, with a value of 2.79 kcal/mol when there is no stimulation, which is approximately 1.84 times larger than the value in the presence of 48.2 THz EM stimulation ($\Delta E_{with} = 1.52$ kcal/mol). This fact illustrates that Na$^+$ is bounded by the -COO$^-$ and is very difficult to exit from the channel. It is concluded that when 48.2 THz EM stimulation is added, Na$^+$ ions undergo kinetic energy transfer and H-bond breaking, the rate increases, and it is easier to break free and leave the channel, thus resulting in an ultrafast permeation rate of Na$^+$.

4. Conclusions

In closing, inspired by the structure of the natural Na$^+$ protein channel, we designed a simple model of a biomimetic sodium channel as a simulated system to investigate the effects of different terahertz EM stimulation on the permeability of the sodium channel. The simulation results elucidated that the EM stimulation at a specific frequency resonating with the functional groups (-COO$^-$) in the channel affects the rate of sodium ions transport across the channel. We conclude that sodium ions permeate more rapidly under 48.2 THz EM stimulation, approaching 33.6 times compared to the normal permeability state. The main mechanism for this phenomenon comes from the interaction between the stimulus

and -COO$^-$ in the channel. As the -COO$^-$ resonantly absorbs the photon energy of the EM stimulation, it then transfers the energy to the Na$^+$ in the channel, increasing the kinetic energy of the ion. By means of the collisions between -COO$^-$, Na$^+$, and water molecules, it breaks the H-bonds between the water and -COO$^-$ in the first aqueous shell layer around the ion, reducing the interaction between the ion and the -COO$^-$, improving the diffusion of the Na$^+$ ions, and reducing the energy consumption. Our findings can be used to improve the transport efficiency of nanofluidic systems [55]; provide some reference value for the detection of diseases of the skeletal system [56], cardiovascular diseases, and other diseases of living organisms [57]; and help to expand the range of applications of EM waves in various fields such as the regulation of neurological diseases [58], energy conversion, and storage. In addition, this mechanism could also serve as an inspiration for promoting life activities with particle transport [59].

Supplementary Materials: The following supporting information can be downloaded at: https://www.mdpi.com/article/10.3390/sym15020427/s1, Figure S1: Schematic representation of an artificial sodium channel; Figure S2: The mean square displacement (MSD) of Na$^+$ ions passing through the channel with and without 48.2 THz electromagnetic stimulation; Figure S3: Probability distribution of the coordination numbers N for Na+ located inside and outside the channels [60–65].

Author Contributions: Conceptualization, Z.Z.; Validation, L.W.; Investigation, Y.Z.; Writing—Original draft, Y.Z.; Writing—Review & editing, Y.L. and Z.Z. All authors have read and agreed to the published version of the manuscript.

Data Availability Statement: The data presented in this study are available in article and supplementary material.

Conflicts of Interest: The authors declare no conflict of interest.

References

1. Hanukoglu, I.; Hanukoglu, A. Epithelial sodium channel (ENaC) family: Phylogeny, structure–function, tissue distribution, and associated inherited diseases. *Gene* **2016**, *579*, 95–132. [CrossRef] [PubMed]
2. Remme, C.A.; Bezzina, C.R. Sodium channel (dys) function and cardiac arrhythmias. *Cardiovasc. Ther.* **2010**, *28*, 287–294. [CrossRef]
3. Sun, P.; Zheng, F.; Zhu, M.; Wang, K.; Zhong, M.; Wu, D.; Zhu, H. Realizing synchronous energy harvesting and ion separation with graphene oxide membranes. *Sci. Rep.* **2014**, *4*, 5528. [CrossRef] [PubMed]
4. Corry, B. Designing carbon nanotube membranes for efficient water desalination. *J. Phys. Chem. B* **2008**, *112*, 1427–1434. [CrossRef] [PubMed]
5. He, Z.; Zhou, J.; Lu, X.; Corry, B. Bioinspired graphene nanopores with voltage-tunable ion selectivity for Na$^+$ and K$^+$. *ACS Nano* **2013**, *7*, 10148–10157. [CrossRef] [PubMed]
6. Koch, S.; Bierbrauer, J.; Haas, K.; Wolter, S.; Grosskreutz, J.; Luft, F.; Spies, C.; Fielitz, J.; Weber-Carstens, S. Critical illness polyneuropathy in ICU patients is related to reduced motor nerve excitability caused by reduced sodium permeability. *Intensive Care Med. Exp.* **2016**, *4*, 10. [CrossRef]
7. Daviet, F.; Blin, M.G.; Fallague, K.; Bachelier, R.; Laforêt, M.; Carré, M.; Poitevin, S.; Dignat-George, F.; Blot-Chabaud, M.; Bardin, N.; et al. Sera from patients with minimal change disease increase endothelial permeability to sodium. *Kidney Int. Rep.* **2020**, *5*, 1071–1075. [CrossRef] [PubMed]
8. Jiang, D.; Shi, H.; Tonggu, L.; El-Din, T.M.G.; Lenaeus, M.; Zhao, Y.; Yoshioka, C.; Zheng, N.; Catterall, W.A. Structure of the cardiac sodium channel. *Cell* **2020**, *180*, 122–134. [CrossRef]
9. Fozzard, H.A.; Makielski, J.C. The electrophysiology of acute myocardial ischemia. *Annu. Rev. Med.* **1985**, *36*, 275–284. [CrossRef]
10. Rush, A.M.; Dib-Hajj, S.D.; Liu, S.; Cummins, T.R.; Black, J.A.; Waxman, S.G. A single sodium channel mutation produces hyper-or hypoexcitability in different types of neurons. *Proc. Natl. Acad. Sci. USA* **2006**, *103*, 8245–8250. [CrossRef]
11. Payandeh, J.; El-Din, T.M.G.; Scheuer, T.; Zheng, N.; Catterall, W.A. Crystal structure of a voltage-gated sodium channel in two potentially inactivated states. *Nature* **2012**, *486*, 135–139. [CrossRef] [PubMed]

12. Naylor, C.E.; Bagnéris, C.; DeCaen, P.G.; Sula, A.; Scaglione, A.; Clapham, D.E.; Wallace, B. Molecular basis of ion permeability in a voltage-gated sodium channel. *EMBO J.* **2016**, *35*, 820–830. [CrossRef] [PubMed]

13. Yang, X.; Zhao, X.; Yang, K.; Liu, Y.; Liu, Y.P.; Fu, W.; Luo, Y. Biomedical applications of terahertz spectroscopy and imaging. *Trends Biotechnol.* **2016**, *34*, 810–824. [CrossRef] [PubMed]

14. Williams, B.S.; Callebaut, H.; Kumar, S.; Hu, Q. 3.4-THz quantum cascade laser based on longitudinal-optical-phonon scattering for depopulation. *Appl. Phys. Lett.* **2003**, *82*, 1015–1017. [CrossRef]

15. Wei, L.; Yu, L.; Jiaoqi, H.; Guorong, H.; Yang, Z.; Weiling, F. Application of terahertz spectroscopy in biomolecule detection. *Front. Lab. Med.* **2018**, *2*, 127–133. [CrossRef]

16. Xiang, Z.; Tang, C.; Chang, C.; Liu, G. A new viewpoint and model of neural signal generation and transmission: Signal transmission on unmyelinated neurons. *Nano Res.* **2021**, *14*, 590–600. [CrossRef]

17. Liu, G.; Chang, C.; Qiao, Z.; Wu, K.; Zhu, Z.; Cui, G.; Peng, W.; Tang, Y.; Li, J.; Fan, C. Myelin sheath as a dielectric waveguide for signal propagation in the mid-infrared to terahertz spectral range. *Adv. Funct.* **2019**, *29*, 1807862. [CrossRef]

18. Sun, L.; Li, Y.; Yu, Y.; Wang, P.; Zhu, S.; Wu, K.; Liu, Y.; Wang, R.; Min, L.; Chang, C. Inhibition of cancer cell migration and glycolysis by terahertz wave modulation via altered chromatin accessibility. *Research* **2022**, *2022*, 986067. [CrossRef]

19. Li, N.; Peng, D.; Zhang, X.; Shu, Y.; Zhang, F.; Jiang, L.; Song, B. Demonstration of biophoton-driven DNA replication via gold nanoparticle-distance modulated yield oscillation. *Nano Res.* **2021**, *14*, 40–45. [CrossRef]

20. Tan, X.; Zhong, Y.; Li, R.; Chang, C. Neuromodulation of Chemical Synaptic Transmission Driven by THz Photons. *Research* **2022**, *2022*, 0010. [CrossRef]

21. Zhang, Q.L.; Yang, R.Y.; Wang, C.L.; Hu, J. Ultrafast active water pump driven by terahertz electric fields. *Phys. Rev. Fluid* **2022**, *7*, 114202. [CrossRef]

22. Pan, Z.; Liu, W.; Yu, L.; Xie, Z.; Sun, Q.; Zhao, P.; Chen, D.; Fang, W.; Liu, B. Resonance-Induced Reduction of Interfacial Tension of Water-Methane and Improvement of Methane Solubility in Water. *Langmuir* **2022**, *38*, 13594–13601. [CrossRef] [PubMed]

23. Yang, R.Y.; Huang, Z.Q.; Wei, S.N.; Zhang, Q.L.; Jiang, W.Z. The resonant heating of heavy water solutions under the terahertz pulse irradiation. *J. Mol. Liq.* **2017**, *229*, 148–152. [CrossRef]

24. Wu, K.; Qi, C.; Zhu, Z.; Wang, C.; Song, B.; Chang, C. Terahertz wave accelerates DNA unwinding: A molecular dynamics simulation study. *J. Phys. Chem. Lett.* **2020**, *11*, 7002–7008. [CrossRef] [PubMed]

25. Cherkasova, O.P.; Serdyukov, D.S.; Nemova, E.F.; Ratushnyak, A.S.; Kucheryavenko, A.S.; Dolhanova, I.N.; Xu, G.; Skorobogatiy, M.; Reshetov, I.V.; Timashev, P.S. Cellular effects of terahertz waves. *J. Biomed. Opt.* **2021**, *26*, 090902. [CrossRef] [PubMed]

26. Zhao, L.; Hao, Y.H.; Peng, R.Y. Advances in the biological effects of terahertz wave radiation. *Mil. Med. Res.* **2014**, *1*, 26. [CrossRef] [PubMed]

27. Zhu, Z.; Chang, C.; Shu, Y.; Song, B. Transition to a superpermeation phase of confined water induced by a terahertz electromagnetic wave. *J. Phys. Chem. Lett.* **2019**, *11*, 256–262. [CrossRef]

28. Zhu, Z.; Chen, C.; Chang, C.; Song, B. Terahertz-Light Induced Structural Transition and Superpermeation of Confined Monolayer Water. *ACS Photonics* **2020**, *8*, 781–786. [CrossRef]

29. Sun, T.; Zhu, Z. Light resonantly enhances the permeability of functionalized membranes. *J. Membr. Sci.* **2022**, *662*, 121026. [CrossRef]

30. Liu, X.; Qiao, Z.; Chai, Y.; Zhu, Z.; Wu, K.; Ji, W.; Li, D.; Xiao, Y.; Mao, L.; Chang, C.; et al. Nonthermal and reversible control of neuronal signaling and behavior by midinfrared stimulation. *Proc. Natl. Acad. Sci. USA* **2021**, *118*, e2015685118. [CrossRef]

31. Hu, Z.H.; Lv, W.P.; Hui, D.X.; Wang, X.J.; Wang, Y.N. Permeability enhancement of the KcsA channel under radiation of a terahertz wave. *Phys. Rev. E* **2022**, *105*, 024104. [CrossRef] [PubMed]

32. Li, Y.; Chang, C.; Zhu, Z.; Sun, L.; Fan, C. Terahertz wave enhances permeability of the voltage-gated calcium channel. *J. Am. Chem. Soc.* **2021**, *143*, 4311–4318. [CrossRef] [PubMed]

33. Guo, L.; Bo, W.; Wang, K.; Wang, S. Theoretical investigation on the effect of terahertz wave on Ca^{2+} transport in the calcium channel. *Iscience* **2022**, *25*, 103561. [CrossRef]

34. Li, Y.; Zhu, Z.; Sun, L.; Xiang, Z.; Chang, C.; Fan, C. Physicochemical Insights on Terahertz Wave Diminished Side Effects of Drugs from Slow Dissociation. *ACS Nano* **2022**, *16*, 8419–8426. [CrossRef] [PubMed]

35. Zhang, Q.L.; Yang, R.Y.; Jiang, W.Z.; Huang, Z.Q. Fast water channeling across carbon nanotubes in far infrared terahertz electric fields. *Nanoscale* **2016**, *8*, 1886–1891. [CrossRef] [PubMed]

36. Zhang, Q.L.; Jiang, W.Z.; Liu, J.; Miao, R.D.; Sheng, N. Water transport through carbon nanotubes with the radial breathing mode. *Phys. Rev. Lett.* **2013**, *110*, 254501. [CrossRef] [PubMed]

37. Payandeh, J.; Scheuer, T.; Zheng, N.; Catterall, W.A. The crystal structure of a voltage-gated sodium channel. *Nature* **2011**, *475*, 353–358. [CrossRef]

38. Kariev, A.M.; Green, M.E. Quantum calculations on ion channels: Why are they more useful than classical calculations, and for which processes are they essential? *Symmetry* **2021**, *13*, 655. [CrossRef]

39. Abraham, M.J.; Murtola, T.; Schulz, R.; Pálla, S.; Smith, J.; Hess, B.; Lindahl, E. GROMACS: High performance molecular simulations through multi-level parallelism from laptops to supercomputers. *SoftwareX* **2015**, *1*, 19–25. [CrossRef]

40. Torrie, G.M.; Valleau, J.P. Monte Carlo free energy estimates using non-Boltzmann sampling: Application to the sub-critical Lennard-Jones fluid. *Chem. Phys. Lett.* **1974**, *28*, 578–581. [CrossRef]

41. Torrie, G.M.; Valleau, J.P. Nonphysical sampling distributions in Monte Carlo free-energy estimation: Umbrella sampling. *J. Comput. Phys.* **1977**, *23*, 187–199. [CrossRef]

42. Allen, T.W.; Andersen, O.S.; Roux, B. Molecular dynamics-potential of mean force calculations as a tool for understanding ion permeation and selectivity in narrow channels. *Biophys. Chem.* **2006**, *124*, 251–267. [CrossRef] [PubMed]

43. Islam, M.A. Einstein-Smoluchowski diffusion equation: A discussion. *Phys. Scr.* **2004**, *70*, 120. [CrossRef]

44. Dill, K.; Bromberg, S. *Molecular Driving Forces: Statistical Thermodynamics in Biology, Chemistry, Physics, and Nanoscience*; Garland Science: New York, NY, USA, 2010.

45. Boulard, B.; Kieffer, J.; Phifer, C.C.; Angell, C.A. Vibrational spectra in fluoride crystals and glasses at normal and high pressures by computer simulation. *J. Non. Cryst. Solids* **1992**, *140*, 350–358. [CrossRef]

46. Lin, S.T.; Blanco, M.; Goddard, W.A., III. The two-phase model for calculating thermodynamic properties of liquids from molecular dynamics: Validation for the phase diagram of Lennard-Jones fluids. *J. Chem. Phys.* **2003**, *119*, 11792–11805. [CrossRef]

47. Du, J.; Xiang, Y. Effect of strontium substitution on the structure, ionic diffusion and dynamic properties of 45S5 bioactive glasses. *J. Non. Cryst. Solids* **2012**, *358*, 1059–1071. [CrossRef]

48. Caine, S.; Heraud, P.; Tobin, M.J.; McNaughton, D.; Bernard, C.C.A. The application of Fourier transform infrared microspectroscopy for the study of diseased central nervous system tissue. *Neuroimage* **2012**, *59*, 3624–3640. [CrossRef]

49. Yang, R.Y.; Jiang, W.Z.; Huo, P.Y. Anisotropic energy absorption from mid-infrared laser pulses in constrained water systems. *J. Mol. Liq.* **2022**, *366*, 120286. [CrossRef]

50. Wojtkowiak, K.; Jezierska, A.; Panek, J.J. Interactions between Artificial Channel Protein, Water Molecules, and Ions Based on Theoretical Approaches. *Symmetry* **2022**, *14*, 691. [CrossRef]

51. Zhu, Z.; Guo, H.K.; Jiang, X.K.; Chen, Y.C.; Song, B.; Zhu, Y.; Zhuang, S. Reversible hydrophobicity-hydrophilicity transition modulated by surface curvature. *J. Phys. Chem. Lett.* **2018**, *9*, 2346–2352. [CrossRef]

52. Guo, Y.W.; Qin, J.Y.; Hu, J.H.; Cao, J.H.; Zhu, Z.; Wang, C.L. Molecular rotation-caused autocorrelation behaviors of thermal noise in water. *Nucl. Sci. Tech.* **2020**, *31*, 53. [CrossRef]

53. Baştuğ, T.; Chen, P.C.; Patra, S.M.; Kuyucak, S. Potential of mean force calculations of ligand binding to ion channels from Jarzynski's equality and umbrella sampling. *J. Chem. Phys.* **2008**, *128*, 04B614. [CrossRef] [PubMed]

54. Ke, S.; Zangerl, E.M.; Stary-Weinzinger, A. Distinct interactions of Na^+ and Ca^{2+} ions with the selectivity filter of the bacterial sodium channel NaVAb. *Biochem. Biophys. Res. Commun.* **2013**, *430*, 1272–1276. [CrossRef] [PubMed]

55. Zhang, Z.; Huang, X.; Qian, Y.; Chen, W.C.; Wen, L.; Jiang, L. Engineering Smart Nanofluidic Systems for Artificial Ion Channels and Ion Pumps: From Single-Pore to Multichannel Membranes. *Adv. Mater.* **2020**, *32*, 1904351. [CrossRef]

56. Wang, H.; Yu, H.; Kim, Y.; Chen, T. Asymmetry in Muscle Strength, Dynamic Balance, and Range of Motion in Adult Symptomatic Hip Dysplasia. *Symmetry* **2022**, *14*, 748. [CrossRef]

57. Esgalhado, F.; Batista, A.; Vassilenko, V.; Russo, S.; Ortigueira, M. Peak Detection and HRV Feature Evaluation on ECG and PPG Signals. *Symmetry* **2022**, *14*, 1139. [CrossRef]

58. Xie, C.; Jauhari, S.; Mora, A. Popularity and performance of bioinformatics software: The case of gene set analysis. *BMC Bioinform.* **2021**, *22*, 191. [CrossRef]

59. Song, B.; Jiang, L. The macroscopic quantum state of ion channels: A carrier of neural information. *Sci. China Mater.* **2021**, *64*, 2572–2579. [CrossRef]

60. Hummer, G.; Rasaiah, J.C.; Noworyta, J.P. Water conduction through the hydrophobic channel of a carbon nanotube. *Nature* **2001**, *414*, 188–190. [CrossRef]

61. York, D.M.; Darden, T.A.; Pedersen, L.G. The effect of long-range electrostatic interactions in simulations of macromolecular crystals: A comparison of the Ewald and truncated list methods. *J. Chem. Phys.* **1993**, *99*, 8345–8348. [CrossRef]

62. Guillot, B.; Guissani, Y. Boson peak and high frequency modes in amorphous silica. *Phys. Rev. Lett.* **1997**, *78*, 2401. [CrossRef]

63. Praprotnik, M.; Janežič, D.; Mavri, J. Temperature dependence of water vibrational spectrum: A molecular dynamics simulation study. *J. Phys. Chem. A* **2004**, *108*, 11056–11062. [CrossRef]

64. Zhu, F.; Hummer, G. Convergence and error estimation in free energy calculations using the weighted histogram analysis method. *J. Comput. Chem.* **2012**, *33*, 453–465. [CrossRef] [PubMed]

65. Kumar, S.; Rosenberg, J.M.; Bouzida, D.; Swendsen, R.H.; Kollman, P.A. The weighted histogram analysis method for free-energy calculations on biomolecules. I. The method. *J. Comput. Chem.* **1992**, *13*, 1011–1021. [CrossRef]